ELSEVIER

Sensors and Actuators B 63 (2000) 138–146

SENSORS AND ACTUATORS B CHEMICAL

www.elsevier.nl/locate/sensorb

Monolithic integrated microfluidic DNA amplification and capillary electrophoresis analysis system

Eric T. Lagally [a], Peter C. Simpson [b,1], Richard A. Mathies [a,b,*]

[a] *UC-Berkeley / UC-San Francisco Joint Bioengineering Graduate Group, University of California, Berkeley, CA 94720, USA*
[b] *Department of Chemistry, University of California, Berkeley, CA 94720, USA*

Abstract

A monolithic integrated DNA analysis system comprised of microfluidic valves and vents, PCR amplification chambers, and capillary electrophoretic separation channels has been microfabricated in a glass sandwich structure. Valves and hydrophobic vents provide controlled and sensorless sample loading into 280 nl PCR chambers; the low volume reactor and the use of thin film heaters permit thermal cycle times as fast as 30 s. The amplified product is labeled with an intercalating fluorescent dye and directly injected into a microfabricated capillary electrophoresis channel. Analyses with this device have produced and detected PCR products from reactions with as few as 20 starting DNA template copies/μl, (five to six copies/chamber). The extrapolated limit of detection based on data using 20 cycles is two copies/chamber. The optimization of heater placement, thermal anisotropy measurements, and the optimization of thermal profiles are also discussed.

Keywords: Monolithic Integration; Microfluidic PCR amplification; Capillary Electrophoresis

1. Introduction

Since the introduction of the polymerase chain reaction, PCR has become one of the most useful and versatile processes in biological science [1]. Amplification of nucleic acids in an exponential fashion is now a major step in most molecular biology applications. However, the amplification process can be slow and inefficient. Most conventional amplification systems rely upon Peltier-effect thermoelectric heating; these systems have a large thermal mass and slow heating and cooling rates, especially when amplifying samples with large volumes (~ 25 μl) encased in containers with low thermal conductivities. Newer systems using heated air circulation around glass capillaries have smaller thermal mass and can therefore be cycled more quickly; however, sample preparation and handling is difficult [2].

Recent work has moved the basic PCR reaction into microfabricated structures. This laboratory produced one of the first microdevices to both amplify and detect PCR products without intermediate steps [3]. This device, comprised of a silicon reaction chamber attached to a glass capillary electrophoresis (CE) separation channel, had a 10-μl volume and performed amplifications in 15 min. Since then, microfluidic PCR devices have been fabricated in silicon [4–7], glass [8,9], silicon-glass hybrids [10], and in fused silica capillaries [11]. Other designs include continuous-flow devices, in which a sample is repeatedly flowed through three differentially heated regions [12], and non-contact methods, in which the IR heat source does not touch the device [13]. Improvements in microreactors have, to date, produced PCR chambers with volumes of order 1 μl and sample concentrations down to roughly 2000 starting copies/μl. Although these devices improve upon conventional thermal cycling systems, most of the reported microreactor amplifications require relatively high starting concentrations [12], a regime in which PCR is non-linear due to reagent-limited losses. Additionally, some of these systems rely upon bulk heating [8,9,13], making parallel analyses with different cycling profiles impossible. To be widely applicable, an integrated amplification and detection system must incorporate individual reactor tempera-

* Corresponding author. Department of Chemistry, 312 Hildebrand Hall, University of California, Berkeley, CA 94720, USA. Fax: +1-510-642-3599.

E-mail address: rich@zinc.cchem.berkeley.edu (R.A. Mathies).

[1] Current address: Kiva Genetics, 2375 Garcia Avenue, Mountain View, CA 94043, USA.

0925-4005/00/$ - see front matter
PII: S0925-4005(00)00350-6

ture control and be capable of amplifying small amounts of template.

The material used to construct the microfluidic PCR device is another important consideration. Silicon is used in the majority of microfabricated reactor designs due to its large thermal conductivity and well-controlled etching properties. However, silicon is more difficult to incorporate into CE and optical detection systems because it is electrically conductive and optically opaque. Glass has proven to be an ideal substrate for CE separations of DNA and other biological molecules [14,15]. Positive characteristics of glass include low native fluorescence, optical transparency, electrical insulation, low cost, and simple microfabrication using wet-etching techniques. These qualities, in addition to being easily coated to provide greatly enhanced results in CE analysis [16,17], also make glass a good substrate for microfabricated PCR reactors. Glass is therefore well-suited to both production of integrated PCR microreactors and CE separation and detection devices.

The development of an integrated DNA amplification and detection system with positive and sensorless microfluidic control is also needed to avoid sample losses through manual handling, to minimize the amounts of reagents, and to place reactants positively in the chamber during thermal cycling. Microreactors open to the environment become increasingly difficult to load manually as the amplification volumes shrink, and thermal gradients induce bubble movement and evaporation causing pumping within the fluid. As a result, completely enclosed chambers are necessary for volumes less than 1 μl. Recent work has demonstrated various methods of implementing the desired fluidic control [18,19]. Anderson et al. [20] developed a microfluidic system comprised of valves (active components) and hydrophobic vents (passive components) in conventionally machined plastic substrates. This system is easily implemented and versatile when operated with volumes in the 1–10-μl range but is not easily extended to submicroliter volume scales.

In this work, we have developed a fully integrated system in glass for the manipulation, amplification, and CE separation of submicroliter volumes of DNA. This system features microfluidic loading and positioning of sample in closed PCR chambers using an active valve and a hydrophobic vent, rapid PCR amplification using thin film heaters, followed by direct injection and rapid separation on a microfabricated CE channel. Experiments to optimize the system design include maximization of temperature uniformity in the chamber and minimization of chamber volume and total cycle time.

2. Experimental section

2.1. Microfabrication

Glass wafers (1.1-mm thick, 100 mm diameter D263, Schott, Yonkers, NY) were cleaned before deposition of an amorphous silicon sacrificial layer (2000 Å) in a low-pressure chemical vapor deposition (LPCVD) furnace. The wafers were primed with hexamethyldisilazane, spin-coated with photoresist (Shipley 1818, Marlborough, MA) at 5000 rpm, and then soft-baked for 30 min at 90°C. The mask pattern was transferred to the substrate by exposing the photoresist in a Quintel UV contact mask aligner. The photoresist was developed in a 1:1 mixture of Microposit developer concentrate and H_2O. The mask pattern was transferred to the amorphous silicon by a CF_4 plasma etch performed in a plasma-enhanced chemical vapor deposition (PECVD) system (PEII-A, Technics West, San Jose, CA). The wafers were etched in a 1:1:2 HF:HCl:H_2O mixture for 7 min at an etch rate of 6 μm/min, giving a final etch depth of 42 μm and a channel width of 100 μm at the bonded surface. The photoresist was stripped and the remaining amorphous silicon removed by a CF_4 plasma etch. Valve and vent structures (see Fig. 1) were formed by drilling a hole to a depth of 965 μm from the back of the etched plate with a 2.5 mm diameter diamond-tipped drill bit (Crystalite, Westerville, OH), using a rotary drill press (Cameron, Sonora, CA). The depth of these holes was controlled using a micrometer attached to the drill, and horizontal alignment was accomplished using a micrometer translation stage. The valve and vent ports were then drilled through the substrate to the channels using a 0.75 mm diameter diamond-tipped bit. The etched and drilled plate was thermally bonded to a 210-μm-thick flat wafer of identical radius in a programmable vacuum furnace at 560°C for 3 h (Centurion VPM, J.M. Ney, Yucaipa, CA). High quality bonds were typically achieved over the entire substrate. After bonding, the channel surfaces were coated using a modified version of the Hjerten coating protocol [16,17]. A more detailed discussion of microfabrication methods is presented elsewhere [21].

Fig. 1 presents the mask design used to create the microfluidic PCR-CE chips. Each valve consists of a main chamber with two smaller fluidic ports within it. One port connects to a common fluidic sample bus, while the other connects to the 0.28-μl PCR chamber. The PCR chamber is connected additionally to the hydrophobic vent port and to the separation system. The separation system consists of a 5-cm-long separation channel connected to three additional ports, the waste, cathode, and anode reservoirs.

A thermal optimization wafer was also constructed which used the same mask pattern as in Fig. 1. This wafer was processed as described above, but was etched in 49% HF to a depth of 250 μm, to permit measurement of the actual chamber temperature with a thermocouple probe inserted through the valve structure into the PCR chamber.

2.2. Fluidics

The valves and vents were controlled by an aluminum manifold depicted in Fig. 2. Each manifold consists of an o-ring set into the base of the manifold that seals the

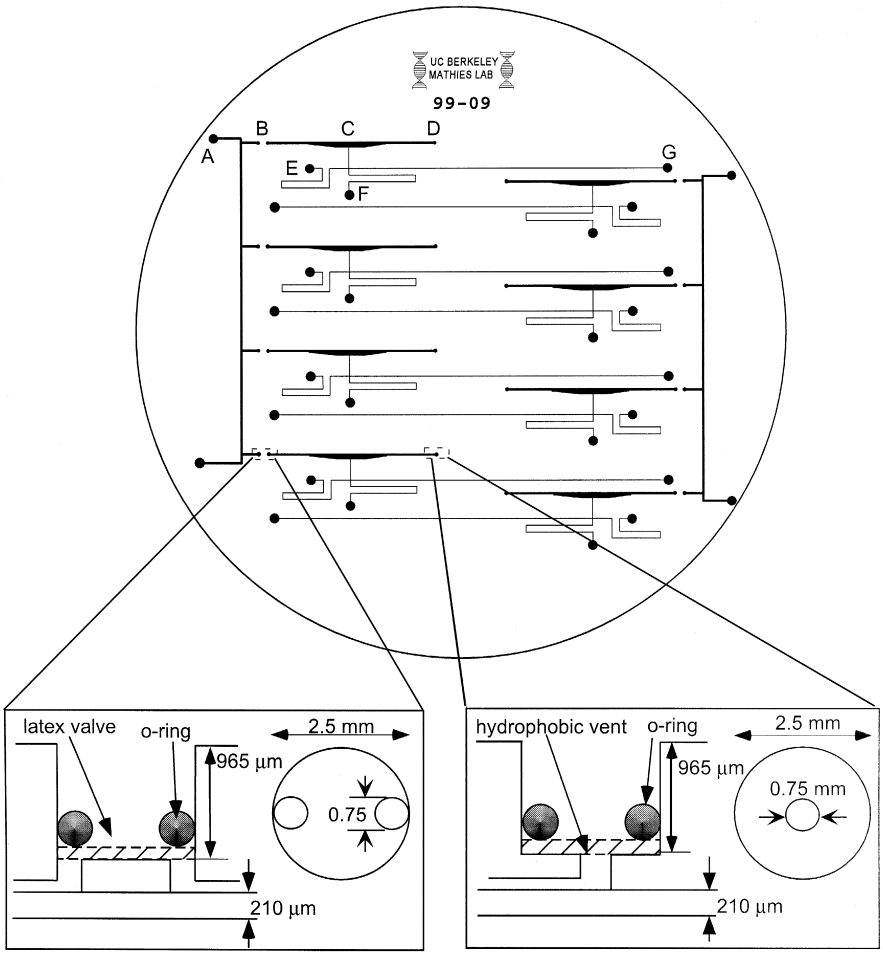

Fig. 1. The 100-mm diameter PCR-CE mask design used in these experiments. The sample is loaded in the fluidic bus reservoir (A); it then travels through the valve port (B) into the 0.28-μl PCR chamber (C), and stops at the vent port (D). The PCR chamber connects directly to the injection cross and separation channel with its cathode (E), waste (F), and anode (G) reservoirs. The insets show the side and top views of the valve and vent structures. This multireactor system permits the introduction of a single sample into four different reactors for multiple analyses if desired.

manifold to the chip when vacuum is applied to the vacuum seal port (V). The ports each have circular projections that fit into the valve/vent structures and seal against o-rings to hold the valve and vent materials in place. Tygon tubing (1/8-in. OD) connects the manifold system via fluidic connectors (Upchurch, Oak Harbor, WA) to a set of computer-controlled solenoid valves that apply vacuum and pressure as required.

Valve and hydrophobic vent materials were installed after fabrication. Latex membranes (2.5 mm diameter, thickness approx. 150 μm) were attached to 2.5 mm ID o-rings (Apple Rubber Products, Lancaster, NY) with epoxy, and the assembly placed around the projections on the valve manifold. Hydrophobic vent material consisting of circular sections of a 1.0-μm-pore size hydrophobic membrane (Millipore, Bedford, MA) was installed similarly.

2.3. Instrumentation

After fabrication, 1-cm diameter heating elements of resistance 7.8 Ω (Minco #HK5537, Minneapolis, MN) and miniature T-type thermocouples (Omega #5TC-TT, Stamford, CT) were applied to the back side of the chip with silicone heat sink compound and secured with polyimide tape. The thermocouple was positioned between the heating elements and the chip. For the thermal optimization experiments, a miniature T-type thermocouple (Omega #5TC-TT) was inserted into the enlarged PCR chamber to measure the temperature within the chamber.

The PCR chambers were thermally cycled with a LabVIEW program (National Instruments, Austin, TX). Thermocouple input voltages passed through a signal conditioning unit (National Instruments) and into a 12-bit ADC card (National Instruments) running on a PowerMacintosh 8500 computer. Temperature control was accomplished through a percentage/integrator/differentiator (PID) module within the LabVIEW program. The DAC output used to control the heater passed through a current source circuit to supply the power necessary to drive the heaters.

During heating, the computer turned on the heater until the temperature of the chamber reached the set point; then the PID maintained the temperature to an accuracy of

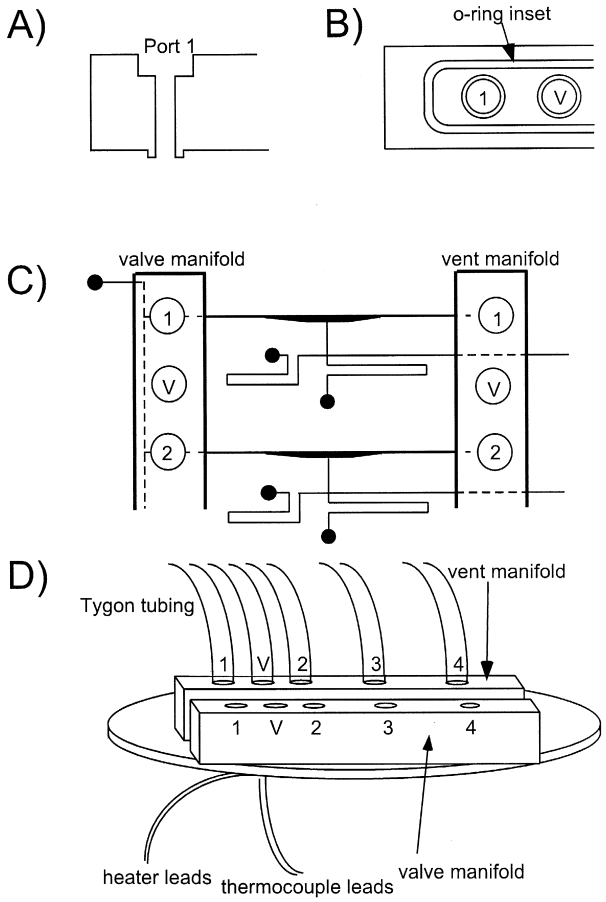

Fig. 2. (A) Cross-sectional, (B) bottom, (C) top and (D) oblique views of the valve and vent block structures. The four ports (1–4) connect external valves to the manifold. The vacuum seal port (V, positioned between the tube ports) is used to hold the manifold to the chip when vacuum is applied.

± 0.5°C. When the amplification cycles were completed, the heater was turned off and the chip was allowed to cool passively. The heater was activated again when the temperature reached the set point and completed the timed step. To speed the cooling steps, a computer fan mounted under the microscope stage was activated by the program at the beginning of each cooling step and deactivated at the end of each cooling step. Nitrogen gas was also flowed over the top surface of the chip during the cooling steps. This equipment allowed for very rapid cooling (~ 10°C/s), resulting in reduced overall cycling times.

Electrophoretic separations were detected with a laser-excited confocal fluorescence detection system as described previously [14]. Briefly, the chip was placed on a stage and the 488-nm line from an argon ion laser was focused on one of the separation channels at a position 4.6 cm from the injection cross. Fluorescence was collected by a 32× (0.4 NA) objective, spatially filtered by a 0.16-mm pinhole, spectrally filtered by a 515-nm bandpass dichroic filter (30-nm band width), and detected by a photomultiplier tube (Products for Research, Danvers, MA).

2.4. Thermal optimization measurements

The thermal cycling profile was optimized to ensure accurate heating of the sample. The only temperature measured during the PCR amplification was the temperature at the heater; correlations between this temperature and the actual chamber temperature were therefore necessary. The 250-μm-deep thermal optimization chip was filled with water and cycled using the thermocouple closest to the heater as the reference thermocouple; the sample thermocouple was placed inside the chamber. Temperature differences between both thermocouples and derivatives of temperature rise were calculated for each temperature step. An adaptive algorithm was used to maximize the rise time derivative and to minimize the temperature difference between thermocouples by adjusting the set parameters of the PID controller after each temperature step.

To optimize the placement of the heating element beneath the PCR chamber, the temperature anisotropy was mapped across the surface of the heater. Using the set-up described above, the thermal optimization chip was filled with water and cycled. The control program captured steady-state temperature data at each of the three temperatures for each cycling run. After each run, the measurement thermocouple was moved horizontally 1.0 mm within the PCR chamber and the run was repeated. The heater was next moved 2.0 mm increments in the lateral direction and the sequence repeated to yield a two-dimensional map of temperature as a function of heater position.

2.5. PCR amplification and electrophoresis

The CE separation medium was 0.75% (w/v) hydroxyethyl cellulose (HEC) in 1× Tris borate EDTA (TBE) buffer with 1 μM thiazole orange. The PCR-CE chips were filled with HEC via the vent reservoir (Reservoir C, Fig. 1) by forcing the solution through the entire microfluidic system using a syringe. The gel was evacuated from the PCR chambers and the sample bus by applying vacuum at the valve reservoir, forming a passive barrier to the flow of reagents from the PCR chamber into the separation channel during amplification. The valve and vent manifolds were sealed to the chip by applying vacuum to the port V (Fig. 2) on each manifold and the sample was introduced at one of the sample bus reservoirs with a pipette. The valve was opened by applying vacuum to the appropriate port on the valve manifold, and vacuum was simultaneously applied to the corresponding hydrophobic vent. Air pressure applied at the sample bus forced the sample through the valve and into the PCR chamber. The valve was then pressure-sealed closed (10–15 psi) to prevent sample movement during heating. Bubble-free loading was consistently achieved using this methodology.

PCR amplification was conducted using a 136 bp amplification product of the M13/pUC19 cloning vector (New England Biolabs, Beverly, MA). The 50-μl PCR

mixture consisted of Taq MasterMix kit (1× PCR buffer, 1.5 mM $MgCl_2$, 200 μM each dNTP, and 2.5 U Taq polymerase, Qiagen, Valencia, CA), 1.5×10^{-5} M BSA, 0.2 μM of each M13/pUC forward and M13/pUC reverse primer (Gibco, Grand Island, NY), and 1×10^3 copies of template DNA. The solution was made fresh daily, divided into two 25-μl aliquots, and kept on ice. The on-chip PCR amplification conditions were 20 cycles of 95°C for 5 s, 53°C for 15 s, and 72°C for 10 s, for a total run time of 10 min. Positive controls were run in a conventional Peltier thermal cycler (MJ Research, Watertown, MA) at the following conditions: 20 cycles of 95°C for 1 min, 53°C for 1 min, and 72°C for 1 min.

The chip was not moved from valve/vent loading through detection; the valve manifold was removed from the chip after PCR to provide access for platinum electrodes and for the placement of 1× TBE run buffer in reservoirs D, E, and F (Fig. 1) for injection and separation. After PCR amplification, 112 V/cm was applied for 10 s between reservoirs C and F to inject the M13 PCR product into the separation channel; separation was performed by applying 236 V/cm between reservoirs E and G (Fig. 1). A DNA sizing ladder, pBR322 *Msp*I (New England Biolabs) was used to verify the size of the PCR product.

3. Results and discussion

Fig. 3 presents the temperature profile as a function of time used for the microfluidic PCR-CE amplification and analysis of M13. The indicated temperature profile is obtained from the standard thermocouple, placed at the heater surface. It was found through consecutive cycling optimization steps (see below) using the thermal optimization chip that this temperature profile gave the most accurate and rapid temperature transitions. As a comparison, the temperature readings within the optimization chip using this heating profile are also indicated on Fig. 3. It was necessary to spike the heater temperature at the beginning of the heating steps to achieve rapid heating within the chamber. The temperature change from the annealing temperature to the extension temperature (72°C) was made slower than the temperature change from extension to denaturing. Longer times were spent between the annealing temperature and the extension temperature to allow extension while preventing primer melting; *Taq* polymerase retains some extension capability even at lower temperatures, whereas at higher temperatures primer strands may melt off the template strand, disrupting amplification [22]. For long extension products, this phenomenon could result in longer extension times, but for short amplification products, even the reduced kinetics of *Taq* polymerase is sufficient to give complete extension.

Fig. 4 presents the temperature of the 250-μm-deep PCR chamber as a function of position across the heater surface. There is notable non-uniformity in the heating

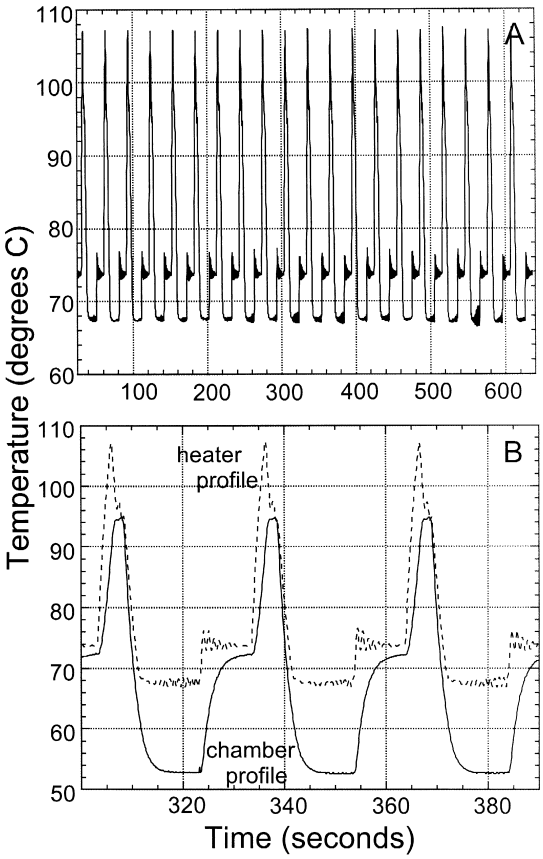

Fig. 3. Thermal cycling amplification profile. (A) The temperature profile at the heater for 20 complete cycles, (B) cycles 10, 11, and 12 of the thermal cycling profile along with the cycling profile within the chamber, obtained using the thermal optimization chip. Dwell times were 5 s at 95°C, 15 s at 72°C, and 10 s at 53°C, for a total run time of 10 min.

across the chamber, especially at the edge. The heater placement used in these experiments was chosen to be 0.2 cm down in the lateral direction and 0.2 cm right in the horizontal direction. The optimum heater placement, defined as the location with the minimum temperature anisotropy, is located at approximately 0.05 cm down and centered in the lateral direction. Our heater placement was selected to provide minimal temperature deviation from the setpoint. The temperatures shown represent an average for each temperature over three amplification cycles. Averaging was done under steady-state conditions by monitoring the final 2 s at 95°C, the final 5 s at 72°C, and the final 10 s at 53°C. Error in these measurements is ±5%, attributed to bubbles and local heating within the optimization chip.

This analysis assumes that the temperatures obtained using the 250-μm-deep thermal optimization chamber accurately represent the temperatures inside the 42-μm-deep PCR chamber. For the reasons given below, we believe that the results presented here are a good approximation to the actual temperature within the chamber. The thermal conductivity of D263 glass at room temperature is 1.07 W/mK [23], almost three times smaller than that of the

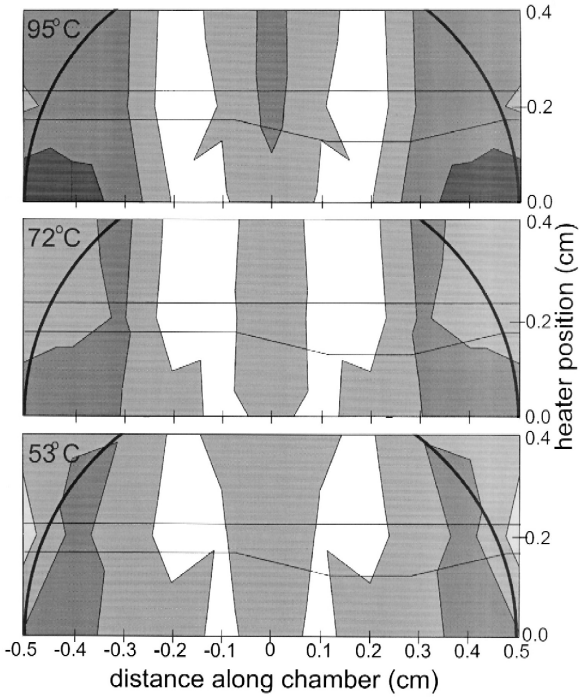

Fig. 4. Contour plot of the average temperature over three cycles for each of the three temperatures used in amplification. The bottom axis indicates thermocouple position across the surface of the heater, where 0.0 cm is the center of the heater. The vertical axis is the distance between the center of the heater and the center of the PCR chamber. The heater and chamber outlines are shown for reference. The temperature below the setpoint was in the 0–5°C □, 5–10°C ▨, 10–15°C (shaded square with X), and 15–20°C ■ ranges.

water within the chamber. Small thermal conductivities result in larger thermal resistances, which decrease heat transfer. Because the bottom glass plate has the smallest thermal conductivity of any material in the device, it is thus the rate-limiting thermal element in the chip. For this reason, the bottom plate used to form the channels in these experiments was chosen to be as thin as possible (210 μm). The top surface of the chip, although thinner in the thermal optimization chip because of the deeper channels etched into it, maintains a characteristic thickness much larger than that of either the bottom plate or the water within the chamber and will not be greatly affected by a change in channel depth. Thus, differences in the top plate thickness can be neglected in a consideration of heat transfer to the sample.

Differences between the thermal optimization chip and the actual cycling device will result in differences in temperature stabilization time; however, these changes are small compared to the length of the cycling profile. According to conductive heat transfer theory, the time required for temperature to reach equilibrium in a stationary material is proportional to L^2/α, where L is the characteristic thickness of a given region and α is the thermal diffusivity. For a change in depth from 42 to 250 μm, the calculated time required to stabilize at temperature (95°C is chosen here to demonstrate the largest change possible) increases from 0.0016 to 0.04 s. Since residence times are two orders of magnitude longer than this, any effect is negligible. The last possible effect of temperature measurement in the thermal optimization chip is heat absorption by the thermocouple within the chamber. It is possible that the chamber temperatures within the cycling chip are actually higher than those reported, since during cycling there is no chamber thermocouple present. The exact level of heat absorption by thermocouples in the chamber is not known. Order of magnitude calculations assuming conductive heat transfer to the thermocouple leads indicate that 5% of the applied heat is transferred to the leads. Temperature differences between the cycling chip and the optimization chip at 95°C averaged 0.6°C, indicating that the optimized PID parameters allowed an effective response to differences between the chips. Additionally, much larger drops in product yield were observed when cycling without the optimized profile, so it is assumed that temperatures measured in the thermal optimization chip are within tolerable error of the actual temperatures within the microfluidic PCR-CE devices.

Fig. 5 presents the results of an analysis of M13 amplicons conducted on the microfluidic PCR-CE chip. The time for performing 20 cycles of amplification is 10 min. After thermal cycling, the PCR product was immediately injected and separated on the electrophoresis channel. No manual transfer of sample was required, and the entire analysis was complete in less than 15 min. The template concentration used in this amplification was 20 copies/μl, resulting in an average of five to six DNA copies in the chamber before amplification. An examination of the signal-to-noise indicates that 20 cycles of amplification yields a S/N ratio of approximately 7:1. Extrapolation to a S/N ratio of 3:1 at this cycle number indicates amplification from only two starting copies in the chamber would be detectable. The use of higher cycle numbers (25–30) to increase the PCR gain would assure detectable signal from a single starting copy in the chamber. Such sensitivity brings this system to the theoretical maximum in sensitivity for PCR amplification.

Fig. 6 plots the electropherogram product peak area for each of four template concentrations. It is expected from the relatively low cycle number and low starting template concentrations that product yield should be a linear function of starting template concentration [24]. The figure demonstrates the expected operation in a regime where reagent-limited losses are insignificant, representing the most powerful amplification possible using this system. Amplification at higher cycle numbers will increase the signal-to-noise, allowing reduction of starting template concentration to single-copy levels, but may decrease linearity. The linearity shown here provides a method for predicting starting template concentration as a monotonic function of product yield, making possible quantitative

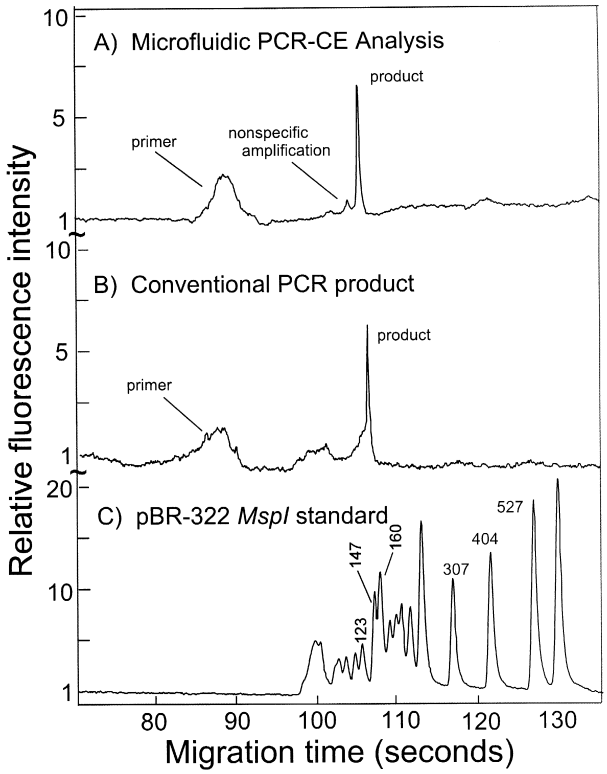

Fig. 5. Microfluidic PCR-CE analysis of an M13 amplicon. The PCR chamber was loaded using back pressure through the valve, to position the sample to be amplified against the hydrophobic vent. Cycling was accomplished using 20 cycles of 95°C for 5 s, 53°C for 15 s, and 72°C for 10 s. (A) Chip PCR-CE analysis of M13 template (20 starting copies/μl, 1× PCR buffer, 1.5 mM $MgCl_2$, 200 μM each dNTP, 2.5 U Taq polymerase, 1.5×10^{-5} M BSA, 0.2 μM M13/pUC forward and M13/pUC reverse primer). (B) Positive control using the identical template solution amplified on a Peltier thermal cycler. (C) pBR322 *Msp*I DNA ladder (15 ng/μl) for size comparison. The positive control and DNA ladder were injected through the PCR chamber in the same manner as the on-chip amplification.

studies of trace target sequences potentially to the single molecule level.

The microfluidic system used for loading and containing the PCR reaction is critical to its success. Previous attempts to conduct PCR using open sample wells or manual loading of the reactor were unsuccessful. Manual loading often resulted in bubbles within the chamber, and open sample wells led to evaporation and sample movement. The major advantage of the present microfluidic system, aside from its ability to transfer small volumes, is that air bubbles are not introduced into the system. The large temperature changes inherent to PCR drive bubble expansion and contraction; any bubble in the chamber will drive sample movement and cause localized heating. If the sample wells are uncovered, evaporation exacerbates this effect. The hydrophobic vent design used by Anderson et al. [20] provides a means for positive, sensorless positioning of the sample during the loading phase. The vent positions the sample and degasses the reaction. The membrane degasses the sample only through diffusion during the PCR reaction, but does provide a slow escape for bubbles should any form during thermal cycling.

The microfluidic PCR-CE chips developed here demonstrate a number of clear advantages over conventional thermal cycling systems and several improvements over recent small-volume PCR systems. First, the volume cycled (0.28 μl) is the smallest to date, which conserves sample and reduces cost. The dead volume of the microfluidic components used here are 50 nl for each valve and 25 nl for each vent. This is an upper bound, however, as not all ports are filled after the initial sample introduction. Small operating volumes also make the device well-suited to rapid cycling: we have demonstrated 20 cycles of PCR amplification in 10 min. The rate-limiting step is the thermal transition time, rather than energy transfer from the heater to the sample. Another significant advantage gained from the small size of the reactor is the improved molecular limit of detection (LOD) observed here: at a given template concentration, there will be fewer template copies in the smaller reactor. The work presented here demonstrates a 100-fold improvement in the LOD compared to the best previous microfabricated thermal cycling reports [10], and up to 10^5 improvement over recently described flow-through designs [12].

The ability to efficiently detect products amplified from low starting concentrations depends in part upon sample injection stacking at the boundary between the PCR chamber and the gel-filled injection channel. The large mobility decrease at this interface results in stacking of the PCR product; as a result, injection times were kept short to avoid overloading the column and fronting effects. One possible limitation of the current design is the non-uniform heating of gel in the injection cross channel. The gel nearest the PCR reactor will be heated more during

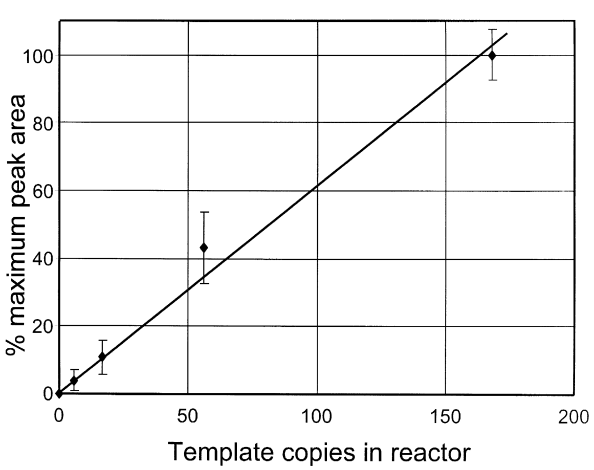

Fig. 6. Plot of amplification product peak area as a function of starting template concentration. For low cycle numbers (i.e., $n < 25$) and relatively small starting template concentrations, reagent-limited saturation is not in evidence and peak area is a linear function of template concentration ($R^2 = 0.9874$).

amplification than the gel nearer the waste reservoir. A small time delay between amplification and injection or the use of smaller or microfabricated heaters more accurately sized to the PCR chamber should reduce or eliminate these temperature-related effects.

Our integrated device eliminates sample handling after the initial loading of the sample bus, which increases assay speed and reproducibility and reduces the possibility of sample contamination from external sources. The entire device is made from inexpensive materials using conventional microfabrication and machining procedures. This reduces the cost of the device, allows for expanded feature density, and also allows the construction of parallel arrays of individually controlled microreactor systems. Future work will include fabrication of thin film heaters on the chip surface with integrated temperature detection; this should further reduce the thermal load, resulting in even faster amplification and improved temperature uniformity across the chamber. Extended applications could include performing multiple PCR reactions and multiplex PCR reactions in parallel on a single device, each using separate thermal cycling profiles, and the performance of thermal cycling-based DNA sequencing. The combination of this PCR-CE technology with current sequencing, forensic and medical assays will create powerful new high-throughput methods for DNA amplification and analysis.

4. Conclusions

A fully integrated microfluidic system to load, PCR amplify, and separate submicroliter volumes of DNA has been constructed for the first time. This system demonstrates positive and controlled microfluidic sample manipulation, coupled to high-speed, high-sensitivity PCR amplification in a completely enclosed and monolithic chamber, directly linked to high-performance microfabricated capillary electrophoretic separation. The sample volume within the PCR chamber (280 nl) is the smallest to date and the resulting sensitivity is two orders of magnitude better than previous microfabricated PCR reactor designs.

Acknowledgements

PCR-CE chip microfabrication was conducted at the University of California, Berkeley Microfabrication Laboratory. ETL gratefully acknowledges the support of a Whitaker Foundation Predoctoral Fellowship. This work was supported as a subcontract to NIST-ATP grant #70NANB5H1031 awarded to Affymetrix and Molecular Dynamics.

References

[1] K. Mullis, F. Faloona, S. Scharf, R. Saiki, G. Horn, H. Erlich, Specific enzymatic amplification of DNA in vitro: the polymerase chain reaction, Cold Spring Harbor Symp. Quant. Biol. 51 (1986) 263–273.
[2] C.T. Wittwer, G.C. Fillmore, D.R. Hillyard, Automated polymerase chain reaction in capillary tubes with hot air, Nucleic Acids Res. 17 (1989) 4353–4357.
[3] A.T. Woolley, D. Hadley, P. Landre, A.J. de Mello, R.A. Mathies, M.A. Northrup, Functional integration of PCR amplification and capillary electrophoresis in a microfabricated DNA analysis device, Anal. Chem. 68 (1996) 4081–4086.
[4] P. Wilding, L.J. Kricka, J. Cheng, G. Hvichia, M.A. Shoffner, P. Fortina, Integrated cell isolation and polymerase chain reaction analysis using silicon microfilter chambers, Anal. Biochem. 257 (1998) 95–100.
[5] A.M. Chaudhari, T.M. Woudenberg, M. Albin, K.E. Goodson, Transient liquid crystal thermometry of microfabricated PCR vessel arrays, J. Microelectromech. Syst. 7 (1998) 345–355.
[6] J.H. Daniel, S. Iqbal, R.B. Millington, D.F. Moore, C.R. Lowe, D.L. Leslie, M.A. Lee, M.J. Pearce, Silicon microchambers for DNA amplification, Sens. Actuators, A 71 (1998) 81–88.
[7] M.A. Northrup, B. Benett, D. Hadley, P. Landre, S. Lehew, J. Richards, P. Stratton, A miniature analytical instrument for nucleic acids based on micromachined silicon reaction chambers, Anal. Chem. 70 (1998) 918–922.
[8] T.B. Taylor, S.E. Harvey, M. Albin, L. Lebak, Y. Ning, I. Mowat, T. Schuerlein, E. Principe, Process control for optimal PCR performance in glass microstructures, Biomedical Microdevices 1 (1998) 65–70.
[9] L.C. Waters, S.C. Jacobson, N. Kroutchinina, J. Khandurina, R.S. Foote, J.M. Ramsey, Multiple sample PCR amplification and electrophoretic analysis on a microchip, Anal. Chem. 70 (1998) 5172–5176.
[10] J. Cheng, M.A. Shoffner, G.E. Hvichia, L.J. Kricka, P. Wilding, Chip PCR: 2. Investigation of different PCR amplification systems in microfabricated silicon-glass chips, Nucleic Acids Res. 24 (1996) 380–385.
[11] N.Y. Zhang, H.D. Tan, E.S. Yeung, Automated and integrated system for high-throughput DNA genotyping directly from blood, Anal. Chem. 71 (1999) 1138–1145.
[12] M.U. Kopp, A.J. de Mello, A. Manz, Chemical amplification: continuous-flow PCR on a chip, Science 280 (1998) 1046–1048.
[13] R.P. Oda, M.A. Strausbauch, A.F.R. Huhmer, N. Borson, S.R. Jurrens, J. Craighead, P.J. Wettstein, B. Eckloff, B. Kline, J.P. Landers, Infrared-mediated thermocycling for ultrafast polymerase chain reaction amplification of DNA, Anal. Chem. 70 (1998) 4361–4368.
[14] A.T. Woolley, R.A. Mathies, Ultra-high-speed DNA fragment separations using microfabricated capillary array electrophoresis chips, Proc. Natl. Acad. Sci. U. S. A. 91 (1994) 11348–11352.
[15] P.C. Simpson, D. Roach, A.T. Woolley, T. Thorsen, R. Johnston, G.F. Sensabaugh, R.A. Mathies, High-throughput genetic analysis using microfabricated 96-sample capillary array electrophoresis microplates, Proc. Natl. Acad. Sci. U. S. A. 95 (1998) 2256–2261.
[16] S.M. Clark, R.A. Mathies, Multiplex dsDNA fragment sizing using dimeric intercalation dyes and capillary array electrophoresis: Ionic effects on the stability and electrophoretic mobility of DNA-dye complexes, Anal. Chem. 69 (1997) 1355–1363.
[17] S. Hjerten, High-performance electrophoresis: elimination of electroendosmosis and solute adsorption, J. Chromatogr. 347 (1985) 191–198.
[18] A. van den Berg, P. Bergveld, in: Micro Total Analysis Systems, Kluwer Academic Publishing, Boston, MA, 1994, pp. 124–135.
[19] M. Esashi, S. Shoji, A. Nakano, Normally closed microvalve and

micropump fabricated on a silicon-wafer, Sens. Actuators 20 (1989) 163–169.
[20] R.C. Anderson, G.J. Bogdan, Z. Barniv, T.D. Dawes, J. Winkler, K. Roy, Microfluidic biochemical analysis system, in: Proc. 1997 International Conference on Solid-State Sensors and Actuators (Transducers '97), Chicago, USA, 16–19 June, 1997, pp. 477–480.
[21] P.C. Simpson, A.T. Woolley, R.A. Mathies, Microfabrication technology for the production of capillary array electrophoresis chips, Journal of Biomedical Microdevices 1 (1998) 7–26.
[22] H.A. Erlich, in: H.A. Erlich (Ed.), PCR Technology: Principles and Applications for DNA Amplification, Freeman, New York, 1989, pp. 1–10.
[23] C. Wimmers, Product Manager, Schott Technical Glass Division, Personal Communication.
[24] S. Schnell, C. Mendoza, Theoretical description of the polymerase chain reaction, J. Theor. Biol. 188 (1997) 313–318.